PNAS RESEARCH ARTICLE | NEUROSCIENCE OPEN ACCESS

Fully-primed slowly-recovering vesicles mediate presynaptic LTP at neocortical neurons

Iron Weichard[a], Holger Taschenberger[b], Felix Gsell[a], Grit Bornschein[a], Andreas Ritzau-Jost[a], Hartmut Schmidt[a], Robert J. Kittel[c], Jens Eilers[a], Erwin Neher[d,e], Stefan Hallermann[a,1], and Jana Nerlich[a,1]

Edited by Thomas Südhof, Stanford University, Stanford, CA; received April 14, 2023; accepted August 26, 2023

Pre- and postsynaptic forms of long-term potentiation (LTP) are candidate synaptic mechanisms underlying learning and memory. At layer 5 pyramidal neurons, LTP increases the initial synaptic strength but also short-term depression during high-frequency transmission. This classical form of presynaptic LTP has been referred to as redistribution of synaptic efficacy. However, the underlying mechanisms remain unclear. We therefore performed whole-cell recordings from layer 5 pyramidal neurons in acute cortical slices of rats and analyzed presynaptic function before and after LTP induction by paired pre- and postsynaptic neuronal activity. LTP was successfully induced in about half of the synaptic connections tested and resulted in increased synaptic short-term depression during high-frequency transmission and a decelerated recovery from short-term depression due to an increased fraction of a slow recovery component. Analysis with a recently established sequential two-step vesicle priming model indicates an increase in the abundance of fully-primed and slowly-recovering vesicles. A systematic analysis of short-term plasticity and synapse-to-synapse variability of synaptic strength at various types of synapses revealed that stronger synapses generally recover more slowly from synaptic short-term depression. Finally, pharmacological stimulation of the cyclic adenosine monophosphate and diacylglycerol signaling pathways, which are both known to promote synaptic vesicle priming, mimicked LTP and slowed the recovery from short-term depression. Our data thus demonstrate that LTP at layer 5 pyramidal neurons increases synaptic strength primarily by enlarging a subpool of fully-primed slowly-recovering vesicles.

synapse | long-term plasticity | presynaptic | vesicle priming | neocortex

Significance

Despite intense investigation, the mechanisms of presynaptic long-term potentiation (LTP) remain poorly understood. This is in part due to an incomplete knowledge of presynaptic function itself. The molecular process of generating fusion-competent synaptic vesicles is referred to as priming. Many of the proteins involved in vesicle priming have long been identified, but only recent studies revealed significant heterogeneity among primed synaptic vesicles (such as normally and superprimed or loosely and tightly docked vesicles). Here, we aimed to analyze presynaptic LTP in light of these recent findings. We show that heterogeneities in vesicle priming must be considered to provide a mechanistic understanding of presynaptic LTP.

Experience-driven strengthening of synapses is the best-understood candidate mechanism mediating learning and memory (1). Long-lasting changes in synaptic strength can be caused by changes in presynaptic neurotransmitter release and/or postsynaptic receptor function. Because presynaptic mechanisms of LTP are less well understood and uncovering their molecular mechanisms and pathways is of fundamental importance for understanding physiological and pathophysiological processes during learning and memory formation (2), presynaptic LTP has been studied intensely in recent years in several brain regions, including hippocampus, neocortex, amygdala, thalamus, and cerebellum (3–5).

For presynaptic LTP observed at large hippocampal mossy fiber boutons, it is generally assumed that induction and expression occur presynaptically (3). However, the underlying mechanisms remain incompletely understood because general aspects of synaptic vesicle priming and fusion and their relation to the regulation of presynaptic function during LTP are still unresolved. Even more limited is our understanding of presynaptic LTP at small conventional boutons mostly exhibiting postsynaptic N-methyl-D-aspartate receptor (NMDAR)-dependent induction of LTP. While the relevance of presynaptic LTP at conventional boutons is still debated (6), it is widely accepted that presynaptic LTP can occur at small conventional boutons exhibiting NMDAR-dependent LTP induction (7, 8) and that it is important for memory formation (2, 3).

A prototypical example of a presynaptic LTP expression at conventional excitatory boutons are the synapses onto neocortical layer 5 pyramidal cells (9–11), where LTP is induced at the postsynaptic site via activation of NMDAR (12–15). At these synapses, an increase in synaptic strength is accompanied by an increase in short-term depression during high-frequency transmission, referred to as redistribution of the synaptic efficacy (9, 16), i.e., synaptic efficacy increases for the first but decreases for subsequent stimuli. An increased probability of release of fusion-competent vesicles (17), also referred to as vesicular release probability (p_{vr}), represents one possible mechanism for such redistribution as it augments early release but attenuates late release due to increased exhaustion of the vesicle pool (9, 17).

Author contributions: E.N., S.H., and J.N. designed research; I.W., H.T., F.G., E.N., S.H., and J.N. performed research; J.E. contributed new reagents/analytic tools; I.W., H.T., F.G., G.B., A.R.-J., H.S., R.J.K., E.N., S.H., and J.N. analyzed data; and H.T., E.N., S.H., and J.N. wrote the paper.

The authors declare no competing interest.

This article is a PNAS Direct Submission.

[1]To whom correspondence may be addressed. Email: hallermann@medizin.uni-leipzig.de or Jana.Nerlich@medizin.uni-leipzig.de.

This article contains supporting information online at https://www.pnas.org/lookup/suppl/doi:10.1073/pnas.2305460120/-/DCSupplemental.

Published October 19, 2023.

Recent advances in our molecular understanding of presynaptic function suggest that vesicle priming is a multistep process resulting in different degrees of priming (18–25). Consistent with this notion, high-resolution structural analyses revealed heterogeneous degrees of tethering and docking of vesicles (26–28), and vesicles residing in such structurally distinct priming states have recently been referred to as loosely and tightly docked vesicles (24) or replacement and docked vesicles (29). However, different priming states have also been observed among vesicles with the same docking distance (30). Furthermore, functional analyses provided evidence for heterogeneous p_{vr} among release-ready vesicles, indicating that heterogeneous vesicle priming and/or heterogeneous p_{vr} give rise to different vesicle subpools referred to as primed and preprimed (31), normally primed and superprimed (32, 33), loosely and tightly docked (34), and replacement and docked vesicles (29). Assuming that these molecular, structural, and functional definitions reflect a common concept that release machinery assembly represents a sequential molecular multistep process giving rise to structurally and functionally distinct vesicle priming states (27), we use here the umbrella term fully-primed when referring to vesicles residing in the higher priming state. The main aim of this study was to analyze the mechanisms of presynaptic LTP in the context of the recent evidence for heterogeneous vesicle priming. Our results show that fully-primed vesicles recover intrinsically slower from synaptic short-term depression and their increased abundance primarily mediates presynaptic LTP at layer 5 pyramidal cell input synapses.

Results

LTP of Excitatory Synapses onto Neocortical Layer 5 Pyramidal Neurons. To study long-term changes in synaptic strength at excitatory synapses onto neocortical layer 5 pyramidal cells, EPSCs were evoked by extracellular stimulation of excitatory inputs (Fig. 1*A*). LTP was induced electrically by pairing extracellular axonal stimulation with postsynaptic suprathreshold depolarization as previously described (9, 10) (Fig. 1*B* and *Methods*). To obtain estimates for release probability and vesicle pool size, paired-pulses and high-frequency stimulations were repeatedly applied before and after LTP induction (Fig. 1*B*). Relative changes in EPSC size ($EPSC_{after}/EPSC_{before}$) observed after stimulation with the LTP induction protocol ranged from 0.64 to 3.32 (n = 39, *SI Appendix*, Fig. S1*A*). A statistically significant increase of the initial EPSC amplitudes was induced in 21 out of 39 cells tested. In the remaining 18 cells, the LTP induction protocol failed to increase EPSC amplitudes ($P > 0.05$ for each cell, referred to as non-inducible connections). Consistently, the average EPSC amplitude across all non-inducible connections was unaltered after stimulation with

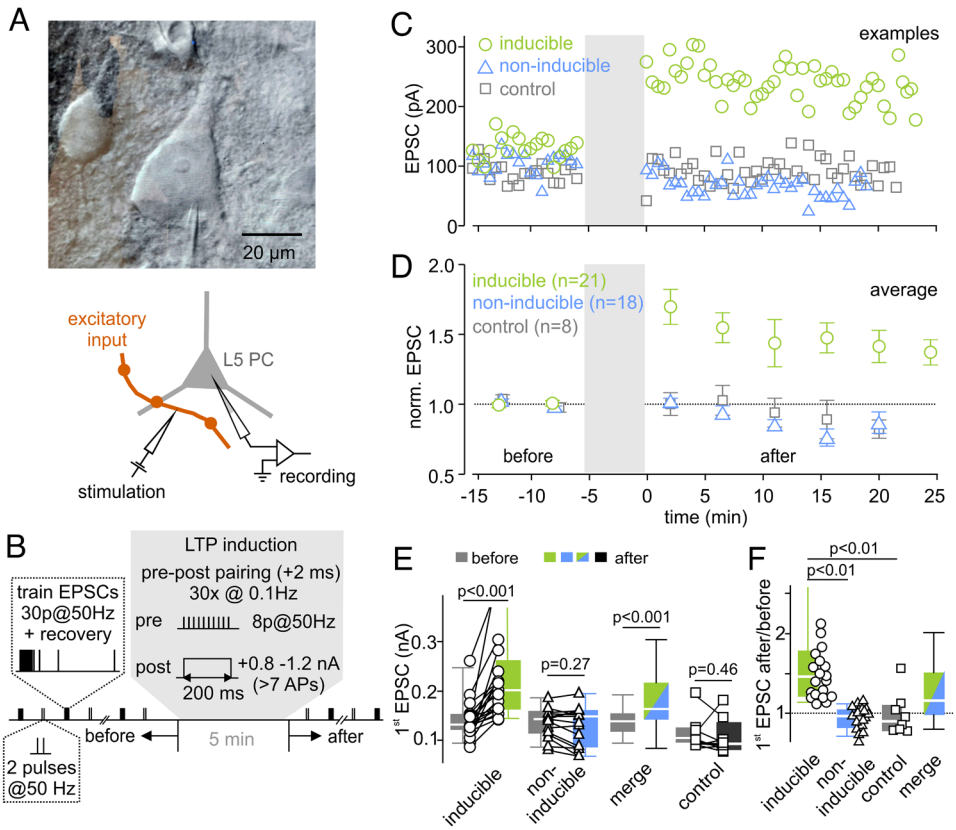

Fig. 1. LTP of excitatory synapses onto neocortical layer 5 pyramidal neurons. (*A*) Infrared DIC image of a patch-clamped layer 5 pyramidal cell (*Top*) and schematic illustration of the recording and stimulation configuration (*Bottom*). (*B*) Illustration of the stimulation protocol used to assess short-term plasticity changes associated with LTP induction in layer 5 pyramidal neurons. Inputs were repeatedly stimulated extracellularly with 50 Hz trains consisting of 30 stimuli followed by single stimuli delivered at various time intervals after a conditioning 50 Hz train to probe recovery from short-term depression. In addition, paired-pulses with 20 ms interstimulus interval were applied after 20 s. This stimulation pattern (train + paired-pulses) was repeated every 45 s for 10 min. To induce LTP, pre- and postsynaptic activities were paired while recording in current-clamp configuration. (*C*) Three example experiments of LTP inducible connections (green), non-inducible connections (blue), and control cells (gray, receiving no LTP induction). (*D*) Normalized mean EPSC amplitudes of inducible connections, non-inducible connections, and control cells before and after LTP induction. (*E*) Individual and median EPSC amplitudes of inducible connections and non-inducible connections, of the merged dataset (inducible and non-inducible connections), and of a control group (no stimulation). (*F*) Box plot and individual data points of the change in EPSC amplitude (after/before) of inducible, non-inducible, and control connections.

the LTP induction protocol (Fig. 1*E*, $P = 0.27$). To analyze the mechanisms underlying EPSC potentiation in more detail, we focused on the experiments with a robust increase in EPSC size (referred to as inducible connections) (Fig. 1).

In inducible connections, the median of EPSC amplitudes increased from 132 pA [124 pA, 151 pA] to 202 pA [164 pA, 251 pA] (median value [first quartile, third quartile]) (Fig. 1*E*), corresponding to a relative increase by 47% [23%, 77%] (Fig. 1*F*; $P < 0.001$; n = 21). Importantly, in the combined dataset of inducible and non-inducible connections, the EPSC amplitude significantly increased after stimulation with the LTP induction protocol ($P < 0.001$; n = 39; Fig. 1*E*) and the relative change of the EPSC size was larger than in unstimulated connections ($P = 0.043$, n = 39, Fig. 1*F* and *SI Appendix*, Fig. S1*B*), excluding the possibility that the increase in EPSC amplitudes in inducible connections was due to selecting cells with randomly increasing EPSC amplitudes. To ascertain stability of recordings, stimulation with the LTP induction protocol was omitted in some cells. These cells showed stable EPSC amplitudes throughout the recording period (control cells, $P = 0.46$, n = 8, Fig. 1 *E* and *F*). Taken together, these data indicate that our protocol of pairing of pre- and postsynaptic activity induces robust LTP in about half of the inputs onto layer 5 pyramidal neurons tested.

EPSCs of inducible and non-inducible layer 5 pyramidal connections had comparable amplitudes and kinetics before LTP induction (*SI Appendix*, Fig. S1*C*), suggesting the recruitment of the same number and type of inputs. Furthermore, short-term plasticity and recovery from synaptic short-term depression (described in more details below) measured before LTP induction were similar in inducible and non-inducible connections (*SI Appendix*, Fig. S1*D*). In paired recordings of synaptically coupled layer 5 pyramidal cells, an increase in synaptic strength after stimulation with the LTP induction protocol was observed in 6 out of 10 cell pairs (*SI Appendix*, Fig. S2, inducible) but not in the remaining four cells (non-inducible). The initial synaptic strength was not different between inducible and non-inducible pairs (inducible = 1.20 ± 0.20 mV, n = 6, non-inducible = 1.03 ± 0.14 mV, n = 4; P = 0.6; range = 0.55–1.93 mV, mean ± SEM, n = 10). Thus, only in a subset of layer 5 - layer 5 connections, LTP was successfully induced under our experimental conditions similar as observed with extracellular axonal stimulation (Fig. 1 and *SI Appendix*, Fig. S2).

LTP Changes Short-Term Plasticity, Increases the Number of Readily Releasable Vesicles, and Slows the Recovery from Synaptic Short-Term Depression. To assess presynaptic mechanisms of LTP, we evaluated changes in short-term plasticity before and after LTP induction by analyzing the EPSC amplitudes during and following high-frequency stimulation (30 stimuli at 50 Hz, Fig. 2 *A* and *B*). Short-term plasticity can also be mediated by postsynaptic mechanisms (35–38). To investigate the contribution of postsynaptic AMPAR saturation and desensitization to short-term plasticity, we recorded EPSCs in response to high-frequency stimulation in the presence of γ-D-glutamylglycine (γDGG, 2 to 3 mM), a low-affinity AMPAR antagonist, attenuating saturation and desensitization (37, 39–42). γDGG reduced the median of the initial EPSC amplitude to 39% [0.27%, 0.41%] (n = 6, *SI Appendix*, Fig. S3*C*) while paired-pulse ratio (PPR), steady-state short-term depression level and time course of recovery from synaptic short-term depression (see below) were unaffected (*SI Appendix*, Fig. S3 *B* and *C*). These data argue against a postsynaptic contribution to changes in short-term depression and rather indicate that short-term plasticity at the stimulated synapses is mediated by presynaptic mechanisms, such as vesicle priming kinetics and pool depletion.

Provided that PPRs are mainly governed by vesicle depletion, changes in PPR may indicate changes in release probability [PPR $\propto (1\text{-}p_{vr})$; but see ref. 34 that PPR and p_{vr} are not necessarily related]. Following LTP induction, PPR decreased by 10% [2.5%, 14%] (median value [first quartile, third quartile]) from 0.85 to 0.77 in inducible connections (Fig. 2*C*, $P = 0.004$, n = 21), but remained unchanged in non-inducible connections ($P = 0.87$, n = 18). Furthermore, relative short-term depression increased after LTP induction in inducible connections as indicated by their smaller normalized steady-state EPSCs amplitudes during high-frequency transmission ($EPSC_{steady\text{-}state}/EPSC_1$). The normalized steady-state EPSC decreased by 20% [13%, 31%] from 0.26 [0.22, 0.35] to 0.21 [0.18, 0.26] ($P \leq 0.001$) in inducible connections but remained unchanged in non-inducible connections ($P = 0.5$) (Fig. 2*E* and *SI Appendix*, Fig. S4). The observed changes in short-term plasticity suggest an increase in the p_{vr} during LTP.

Both the initial EPSCs and also the absolute steady-state EPSCs of high-frequency EPSC trains were potentiated following LTP induction (cf. Fig. 2*D*). A sole redistribution of synaptic efficacy (i.e., an exclusive increase in p_{vr}) cannot account for the observed increase in steady-state EPSCs. Alternatively, larger steady-state EPSCs during sustained high-frequency transmission could be caused by an increased size of the readily releasable pool of synaptic vesicles. To assess RRP changes, we relied on established analyses methods using cumulative EPSC amplitudes (*SI Appendix*, *Methods*). Two approaches to estimate RRP size (43) indicated an increase between 7% and 30% in inducible connections (7% [0%, 31%] with the Elmqvist–Quastel method [EQ], $P = 0.045$, n = 17, Fig. 2*G*; and 30% [15%, 54%] with the Schneggenburger–Meyer–Neher method [SMN], $P \leq 0.001$, n = 21, Fig. 2*F*). These data suggest that an enlargement of the RRP contributes to LTP expression. The RRP size was unchanged in non-inducible connections (Fig. 2 *F* and *G* and *SI Appendix*, Fig. S4 *B* and *C*; SMN method: $P = 0.3$, EQ method $P = 0.99$). Alternatively, increased quantal size may contribute to elevated steady-state amplitudes. This is difficult to measure specifically for synapses undergoing potentiation. We therefore measured spontaneously occurring EPSCs before and after pharmacological potentiation of all synaptic inputs to approximate quantal size (see below).

In addition, we observed changes in the recovery from short-term depression (Fig. 2*H*). The recovery from short-term depression provides valuable information on the mechanisms of vesicle priming. Particularly, the number of exponential components and their relative contribution and time constant may reflect heterogeneity of vesicle priming and reveal details about the kinetics of vesicle priming (44). The recovery time course was therefore fit with either a mono- or biexponential function (for criteria, see *SI Appendix*, *Methods*) yielding either a single (τ_{mono}) or two time constants (τ_{fast} and τ_{slow}) with corresponding fractional amplitudes. In case of biexponential fits, a weighted time constant (τ_{wd}) was calculated for comparison to single-exponential fits (cf. *SI Appendix*, Methods). In inducible connections, the median recovery time constant increased ~fivefold from 0.35 s [0.22 s, 0.81 s] before to 1.61 s [0.74 s, 2.58 s] after LTP induction (Fig. 2*I*, $P \leq 0.001$, n = 19). Before LTP induction, the EPSC recovery time course was best fit with a monoexponential function in the majority of cells (Fig. 2*J*, τ_{mono} = 0.25 s [0.21 s, 0.38 s], n = 14). After LTP induction, the recovery time course was best fit with a biexponential function in nearly all inducible connections. In a majority of cells, an additional slow recovery component emerged after LTP

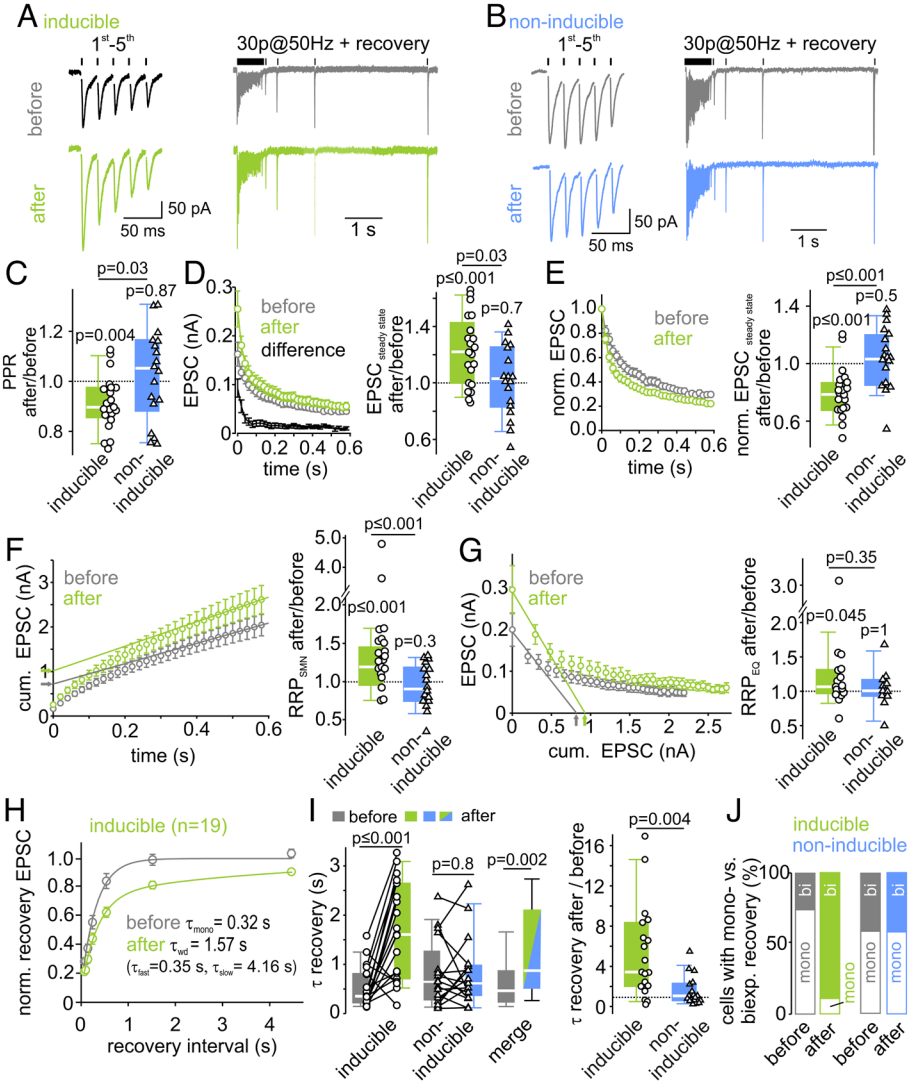

Fig. 2. LTP changes short-term plasticity, increases the number of readily releasable vesicles, and slows the recovery from synaptic short-term depression. (*A* and *B*) Example average traces of the first 5 EPSCs (*Left*) of a 50-Hz-EPSC train (*Right*), followed by EPSCs elicited by single stimuli at different interstimulus intervals to probe recovery from short-term depression, recorded before (*Top*, gray) and after (*Bottom*, green or blue) LTP induction in inducible (*A*) and in non-inducible (*B*) connections. (*C*) Individual and median relative changes in PPR after LTP induction in inducible and non-inducible connections. (*D*) Mean EPSC amplitudes during 50-Hz-trains were increased after LTP induction in inducible connections (*Left*). The difference curve indicates an increased synaptic strength throughout the train with a higher potentiation for the first EPSCs in inducible connections. (*Right*) Relative changes of steady-state EPSC amplitudes after LTP induction in both inducible and non-inducible connections. (*E*) Mean normalized high-frequency EPSCs exhibit short-term depression, which increased in inducible connections after LTP induction. (*F*) RRP size estimation by back-extrapolation of a linear fit to the last five amplitudes of the cumulative EPSC train plotted as a function of stimulus time (SNM method) shows an increase in inducible connections (*Left*). Relative changes of RRP size after LTP induction for inducible and non-inducible connections are shown in the *Right* panel. (*G*) RRP size estimation by forward-extrapolation of a linear fit to the first three amplitudes of the EPSC train plotted as a function of cumulative previous release (EQ method) also shows an increase after LTP induction in inducible connections. Relative changes of RRP size after LTP induction for inducible and non-inducible connections are shown in the *Right* panel. (*H*) Mean normalized EPSCs during recovery from short-term depression plotted as a function of recovery interval reveal a slower recovery from synaptic short-term depression after LTP induction in inducible connections. The time constants of recovery from short-term depression were calculated from either mono- or biexponential fits to the mean recovery time course (lines). (*I*) Comparison of individual and median absolute (*Left*) and summary plot of relative changes (*Right*) of the weighted recovery time constant reveals a slowing of recovery from short-term depression after LTP induction in inducible (n = 19) but not in non-inducible connections (n = 17). (*J*) Proportion of cells (in %) with a mono- or biexponential recovery before and after LTP induction in inducible and non-inducible connections. Before LTP induction, a majority of the inducible connections exhibits a monoexponential recovery time course. After LTP induction, nearly all inducible connections exhibit a biexponential recovery from short-term depression.

induction (τ_{slow} = 4.39 s [1.98 s, 6.52 s], n = 17), while τ_{fast} obtained from the biexponential fit was similar to τ_{mono} obtained from the monoexponential fit before LTP (τ_{fast} = 0.31 s [0.24 s, 0.43 s], n = 17; τ_{mono} before vs. τ_{fast} after LTP P = 0.46). In five cells, EPSCs recovered biexponentially already before LTP. When comparing τ_{slow} values before and after LTP induction in these five cells (paired) or pooled τ_{slow} values before and after LTP induction (unpaired) we did not detect a significant difference (τ_{slow} before = 2.33 s [1.78 s, 4.63 s], n = 5 vs. τ_{slow} after = 5.02 s [2.86 s, 6.41 s] n = 5, paired Wilcoxon test P = 0.13; τ_{slow} before 2.33 s [1.78 s, 4.63 s] vs. τ_{slow} after = 4.39 s [1.98 s, 6.52 s] n = 17, unpaired Mann–Whitney U test P = 0.39). Based on these observations, we conclude that the increase of τ_{wd} following LTP induction is caused by an increase in the relative contribution of the slow recovery component. The recovery from synaptic short-term depression in non-inducible connections was unaffected by the LTP induction protocol (Fig. 2 *I* and *J* and *SI Appendix*, Fig. S4). These findings are

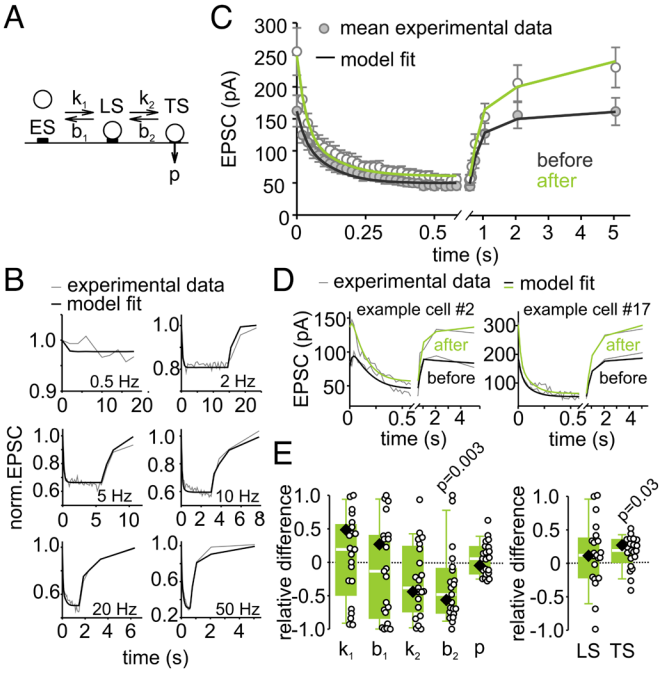

Fig. 3. A sequential two-step priming model indicates an increased number of tightly docked vesicles following LTP induction. (*A*) Sequential model containing empty sites (ES), loosely docked vesicles (LS), and fusion-competent tightly docked vesicles (TS). (*B*) Model fit to average EPSC trains recorded in response to various stimulation frequencies. (*C*) Model fit to the mean 50-Hz EPSC train and the recovery EPSCs recorded in inducible connections before and after LTP induction. (*D*) Model fits to individual 50-Hz EPSC trains and recovery EPSCs before and after LTP induction in two example cells. (*E*) LTP-induced individual (circles) and median relative differences (eq. 7 in *SI Appendix*, Methods) of the predicted model parameters (diamond = parameter obtained from model fit to the average of all inducible connections). *P* values were calculated by comparison of respective parameters before and after LTP induction by Wilcoxon-signed rank tests.

reminiscent of the previously observed additional slow component of recovery upon superpriming of vesicles with the GTP-binding protein Rab3 (32). In sum, the data show that recovery from synaptic short-term depression occurs substantially slower after LTP induction due to a more prominent slow recovery component, consistent with the hypothesis of an LTP-induced augmentation of a subpool of fully-primed slowly-recovering vesicles.

Sequential and Parallel Models of Vesicle Priming Reproduce Experimentally Observed Short-Term Plasticity. To evaluate changes in vesicle priming after LTP induction more quantitatively, we tried to reproduce our experimental data in numerical simulations using two validated models of vesicle priming and fusion based on either parallel or sequential kinetic schemes. First, we tested a model in which release can originate from two parallel pathways represented by two types of fusion-competent vesicles states: high-p_{vr} vesicles, which recover slowly, and low-p_{vr} vesicles, which recover rapidly (*SI Appendix*, Fig. S5*A*; referred to as "parallel model" in the following (45)). This model evolved from analyses of models with increasing complexity (46–48). High-p_{vr} vesicles can be considered as being analogous to previously described "superprimed vesicles" (32, 33). In addition, a limited supply pool of vesicles is assumed (N_0, ref. 46). Because high-p_{vr} vesicles intrinsically recover slowly, addition of high-p_{vr} vesicles after LTP induction can explain not only the observed increased EPSC amplitude and increased relative steady-state short-term depression but also the slower recovery of EPSCs following high-frequency trains.

In addition, we tested a model that assumes two vesicle states (referred to as TS and LS for tightly and loosely docked states, respectively) of which only TS vesicles are fusion-competent (Fig. 3*A*; referred to as "sequential model" in the following (45)). This model faithfully reproduces several short-term plasticity features experimentally observed at calyx of Held synapses; refs. 34 and 49). The recruitment of vesicles into LS and the transition from LS to TS is mediated by Ca^{2+}-dependent rate constants. The LS to TS transition is slow at rest, but increases linearly with $[Ca^{2+}]_i$, such that each AP shifts a certain fraction of vesicles from LS to TS. The equilibrium between vesicles in states LS and TS at rest determines initial EPSC amplitudes. The balance between release of TS vesicles and their resupply determines the degree of the initial short-term depression including the PPR. A shift in the equilibrium between vesicles states at rest in favor of TS accounts for the observed increased EPSC amplitude and enhanced relative steady-state short-term depression after LTP induction. The need to convert a higher proportion of vesicles from LS to TS (after depletion of TS vesicles) leads to a larger slow component of EPSC recovery and its overall slowdown.

We first compared the ability of the models to reproduce short-term depression during stimulus trains at frequencies ranging from 0.5 to 50 Hz and the subsequent recovery from short-term depression. After optimization of the free parameters, both models reproduced short-term depression time courses well. The sequential model performed slightly better compared to the parallel model (Fig. 3*B* and *SI Appendix*, Fig. S5*B*; χ^2 = 15.97 and 19.34 for sequential and parallel model, respectively). We therefore show the results of the sequential and parallel model in main and supplementary figures, respectively. The experimental data available do not allow us to unambiguously favor one model over the other because both models are able to reproduce our experimental findings almost equally well (50).

Both Models Indicate a Selective Enlargement of a Vesicle Subpool Following LTP Induction. Next, we optimized a subset of the five free parameters of both models (*SI Appendix*, *Methods*) to faithfully reproduce short-term plasticity before and after LTP induction observed for the average response across all inducible connections (Fig. 3*C* and *SI Appendix*, Fig. S5*C*). In addition, we also optimized the free parameters for each of the 21 connections individually (see Fig. 3*D* and *SI Appendix*, Fig. S5*D* for two examples). We then compared the best-fit parameters of the sequential model before and after LTP induction for each synaptic connection and plotted the relative differences or the ratios (Fig. 3*E* and *SI Appendix*, Fig. S7 *B* and *E*; see equation 7 in *SI Appendix*, Methods). This parameter comparison indicates a reduction of b_2, the rate constant of the backward transition LS←TS, which can be interpreted as an LTP-induced stabilization of the TS state resulting in a higher occupancy of the TS state at rest (see equations 5 and 6 in *SI Appendix*, *Methods*; Fig. 3*E*). In analogy, the number of high-p_{vr} vesicles (N_2) increased when analyzing LTP-induced changes in short-term plasticity with the parallel model (*SI Appendix*, Fig. S5*E*). When non-inducible connections were subjected to the same analysis, no significant differences in model parameters before and after LTP induction were found (*SI Appendix*, Fig. S4 *D–I*). Thus, an unbiased parameter optimization for two mechanistically different short-term plasticity models revealed a selective increase in the number of fully-primed slowly-recovering vesicles (which are referred to as TS vesicles in the sequential and N_2 vesicles in the parallel model).

To corroborate that our results can be reproduced by assuming heterogeneous priming of subpools of vesicles, we used a linear unmixing-approach (*SI Appendix*, Methods) in which release time

courses during high-frequency trains observed in each of the 21 connections before and after LTP induction are described by a linear combination of components representing the release time courses of the distinct vesicle subpools preexisting at the onset of stimulation. We observed an exclusive increase in the TS component in the sequential and the N_2 component in the parallel model upon inducing LTP (*SI Appendix*, Fig. S6). These data therefore provide additional support for our hypothesis that LTP is mediated by a selective augmentation of the subpool of fully-primed slowly-recovering vesicles.

Stronger Synapses Recover more Slowly from Short-Term Depression. At the calyx of Held synapse, stronger synapses were shown to exhibit stronger paired-pulse depression (i.e., lower PPR), which was interpreted as a higher fraction of fully-primed vesicles [superpriming (33) or higher fraction of TS vesicles (34)]. PPRs and initial EPSC sizes in layer 5 pyramidal cells obtained before LTP induction show a similar correlation (gray + black points in Fig. 4*A*; $P = 0.007$). The PPRs and initial EPSC sizes obtained after LTP induction appeared to be shifted along the regression line to the data obtained before LTP induction or at least to be shifted in a similar direction (cf. arrows in Fig. 4 *A*, *C*, and *E*). Since this correlation was previously associated with superpriming or a shift in the LS-TS balance, these data are consistent with the assumption of fully-primed vesicles mediating LTP-induced enhancement of synaptic strength. In addition, we observed correlations between the degree of short-term plasticity, such as PPR and the kinetics of recovery from short-term depression in control data (control = all connections before plasticity induction, gray and black points in Fig. 4*C*, $P < 0.0001$). Consistently, the recovery from short-term depression slows with increasing EPSC size (gray and black points in Fig. 4*E*, $P = 0.038$). Note, we had to exclude five cells from scatter plots against absolute EPSC size (Fig. 4 *A* and *E*), which had been obtained at a higher stimulus intensity resulting in much higher amplitudes. Again, the respective data obtained after LTP induction appeared to be shifted along the regression line to the data obtained before LTP induction. In conclusion, these observations are consistent with our hypothesis that LTP induction primarily leads to a larger abundance of slowly-recovering vesicles or else shifting the LS ↔ TS equilibrium at rest toward TS.

To explore possible mechanisms that may account for these correlations between PPR vs. EPSC size and τ recovery vs. PPR, we systematically varied the free parameters of our two models during simulations. The two correlations were best predicted by varying b_2 (LS←TS backward transition rate constant) in the sequential (*SI Appendix*, Fig. S7*C*) and by varying N_2 (size of the superprimed vesicle pool) in the parallel model (*SI Appendix*, Fig. S7*E*) but less well by varying any of the other free model parameters. These data indicate that the two analyzed correlations can only be explained by changing the abundance of TS vesicles in the sequential model (determined by the $k_{2,rest}/b_2$ ratio) and by the number of superprimed vesicles (N_2) in the parallel model, providing additional quantitative support to the notion that addition of fully-primed and slowly-recovering vesicles (TS or N_2 vesicles) can explain both the variability among control synapses and their potentiation following LTP induction.

To establish whether these findings extend beyond excitatory inputs to cortical layer 5 pyramidal neurons, we analyzed data from other synapses. We observed similar correlations in hippocampal Schaffer collateral to CA1 pyramidal neuron synapses (Fig. 4*G*) and synapses between cultured neocortical neurons (Fig. 4 *H* and *I*), not only with respect to the functional heterogeneity among synapses under control conditions (black symbols) but also with respect to changes evoked by electrically and pharmacologically induced plasticity, and by induction of homeostatic plasticity (magenta symbols). These data suggest that the abundance of fully-primed and slowly-recovering vesicles

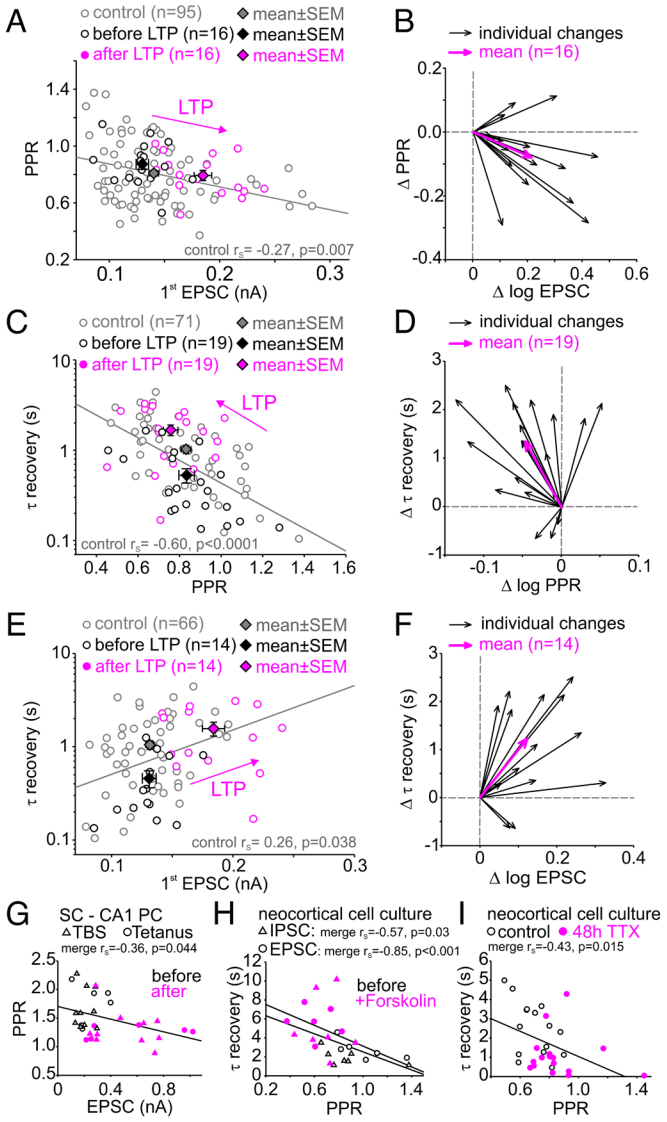

Fig. 4. Stronger synapses recover more slowly from short-term depression. (*A*) Scatter plot of PPR vs. first EPSC amplitude in layer 5 pyramidal cells before and after LTP induction. (*B*) Vector plot showing individual (black arrows) and average (magenta arrows) changes in EPSC size and PPR for inducible connections (n = 16). (*C*) Scatter plot of the time constant of recovery from synaptic short-term vs. PPR before and after LTP induction. (*D*) Vector plot showing individual (black arrows) and average (magenta arrows) changes of recovery from short-term depression and PPR of inducible connections (n = 19). (*E*) Scatter plot of time constant of recovery from synaptic short-term depression vs. EPSC amplitude before and after LTP induction. (*F*) Vector plot showing individual (black arrows) and average (magenta arrows) changes of first EPSC amplitude and recovery from synaptic short-term depression of inducible connections (n = 14). (*G*) Scatter plot of PPR vs. EPSC size (cf. Fig. 4*A*) before and after plasticity induction by theta burst (TBS)- or tetanic stimulation of Schaffer collateral to CA1 pyramidal cell synapses in acute brain slices. (*H*) Scatter plot of time constant of recovery vs. PPR (cf. Fig. 4*B*) for high-frequency (20 pulses at 20 Hz) IPSC (triangles) and EPSC (circles) trains before and during forskolin application in synapses of cultured neocortical neurons. (*I*) Scatter plot of time constant of recovery vs. PPR (cf. Fig. 4*B*) for control high-frequency IPSC trains (20 pulses at 50 Hz) and after induction of homeostatic plasticity by inactivity (48 h TTX) in synapses of cultured neocortical neurons. Note, the homeostatic plasticity-induced shift of IPSCs toward larger PPR and faster recovery from short-term depression.

critically determines synapse-to-synapse variability of synaptic strength and short-term plasticity. Note that the correlation between steady-state short-term depression and τ recovery could not be assessed for hippocampal Schaffer collateral to CA1 pyramidal cell synapses in acute slices, which showed synaptic facilitation. Furthermore, the correlation between initial EPSC size and PPR could not be assessed for cultured neurons, which showed highly variable EPSC sizes within the pooled control and potentiated cell group.

Forskolin- and PDBu-Induced Potentiation Slows Recovery from Short-Term Depression. To further test our hypothesis of enhanced vesicle priming following LTP induction, we potentiated synapses by stimulating the cAMP or DAG pathway (Fig. 5*A*) via application of the adenylate cyclase activator forskolin or the DAG analog PDBu. These two pharmacological manipulations have been shown to stimulate vesicle priming by modulation of active zone priming proteins including RIM1α and Munc13, and thereby inducing an increase in synaptic strength (*Discussion*).

We first analyzed spontaneously occurring EPSCs (sEPSCs) before and during bath application of 40 μM forskolin or 1 μM PDBu (Fig. 5*B*). The median frequency of the sEPSCs increased by 16% [0%, 36%] following forskolin application and by 38% [12%, 52%] following PDBu application (Fig. 5 *C*, *Left*, $P = 0.008$, n = 21; $P = 0.012$, n = 9; respectively), consistent with increased release because of higher release probability and/or increased number of docked vesicles (51). In addition, sEPSCs amplitudes increased after forskolin and PDBu treatment by a

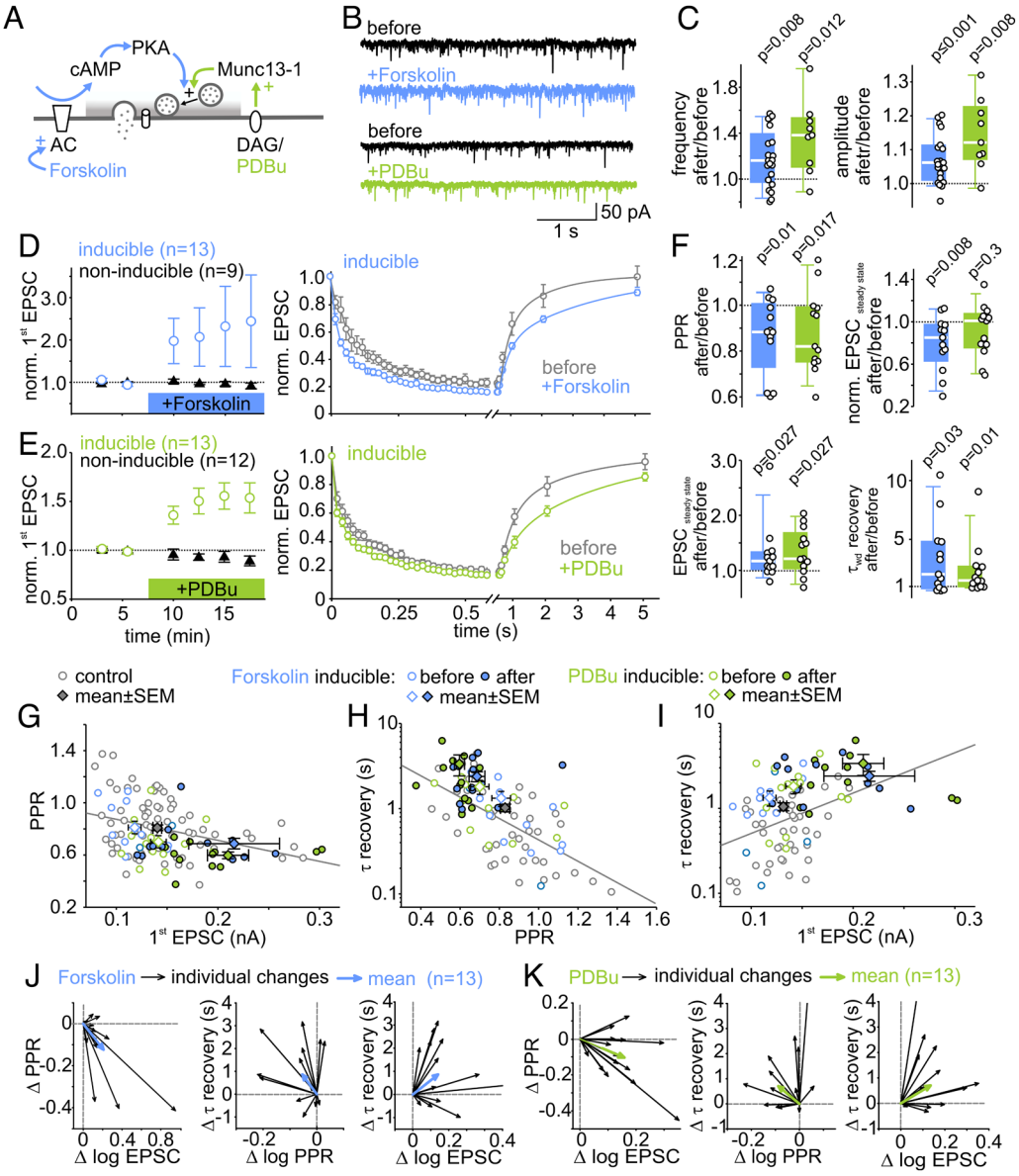

Fig. 5. Forskolin- and PDBu-induced potentiation slows recovery from short-term depression. (*A*) Schematic of forskolin- and PDBu-activated signaling pathways. (*B*) Example traces of spontaneous EPSCs (sEPSCs) before (black) and after (colored) forskolin or PDBu application. (*C*) Individual and median relative changes in sEPSC frequency (*Left*) and amplitude (*Right*) before and after forskolin or PDBu application. For sEPSC analysis, data from inducible and non-inducible connections were pooled. (*D* and *E*) Mean normalized initial EPSC amplitudes of inducible and non-inducible connections (*Left*) and mean normalized 50-Hz EPSC trains and recovery EPSCs of inducible connections (*Right*) before and during forskolin (*D*) or PDBu (*E*) application. (*F*) Individual and mean relative changes in PPR, absolute and normalized steady-state EPSC amplitudes, and recovery time constant in inducible connections after forskolin or PDBu application. (*G*–*I*) Scatter plot of PPR vs. initial EPSC (*G*, two data points out of range), recovery from short-term depression vs. PPR (*H*, one data point out of range), and recovery from short-term depression vs. EPSC size (*I*, three data points out of range) before and after potentiation by forskolin (n = 13) and PDBu (n = 13) (control data same as in Fig. 4 *A*, *C*, and *E*, respectively). (*J* and *K*) Vector plots showing individual (black arrows) and average (blue arrows) changes in PPR and EPSC size (*Left*), PPR and recovery from short-term depression (*Middle*), and recovery from short-term depression and EPSC size (*Right*) for forskolin (*J*) and PDBu (*K*) inducible connections.

median percentage change of 6% [0%, 11%] ($P < 0.001$, n = 21) and 12% [1%, 22%] ($P = 0.008$, n = 9), respectively (Fig. 5 *C*, *Right*). The median amplitude of the sEPSCs was 15.2 pA [13.4 pA, 16.1 pA] (n = 30) under control conditions, which is comparable to previously reported amplitudes of spontaneously fusing vesicles (mEPSCs) (52). Assuming that the majority of sEPSCs represent mEPSCs, the quantal size increased by ≤6 to 12%. However, the reliability of this assessment of the extend of a postsynaptic contribution to synapse strengthening is limited, and spontaneous and evoked neurotransmitter release might be mediated by different vesicle populations (53). Nevertheless, our data are consistent with the view that pharmacologically induced potentiation is predominantly presynaptic in origin.

To evaluate the presynaptic mechanisms of pharmacologically induced synapse potentiation, EPSCs (30 pulses at 50 Hz + recovery EPSCs) were repeatedly measured before and during bath application of forskolin or PDBu and analyzed with respect to changes in short-term synaptic plasticity and recovery from synaptic short-term depression. Similar to LTP induced by electrical stimulation (cf. Figs. 1 and 2), in approximately half of the cells (inducible connections), pharmacological stimulation induced robust EPSC potentiation by 38% [27%, 56%] (n = 13) and 37% [28%, 52%] (n = 13), respectively (Fig. 5 *D* and *E*), while in the remainder of the cells tested, EPSC amplitudes remained unchanged (non-inducible connections). The fractions of cells exhibiting EPSC potentiation were similar for the different modes of plasticity induction (LTP = 54%, forskolin-potentiation = 59%, PDBu-potentiation = 52%).

Strikingly, analysis of short-term plasticity during EPSC trains revealed decreased PPR and slower recovery from short-term depression after pharmacological potentiation (Fig. 5*F*), similar as observed for LTP induced by electrical stimulation (cf. Fig. 2). Short-term depression during high-frequency transmission was only increased after forskolin but not after PDBu application. Consistently, correlations as shown for LTP induced by electrical stimulation were observed for pharmacologically induced potentiation (Fig. 5 *G*–*K*; cf. with Fig. 4 *A*–*F*). These data indicate that irrespective of the mode of induction, potentiation of synaptic strength is accompanied by increased relative short-term depression and by a slowing of recovery after high-frequency transmission.

Discussion

To investigate presynaptic mechanisms of LTP, we analyzed short-term plasticity before and after LTP induction at excitatory synapses onto cortical layer 5 pyramidal neurons. LTP induction by paired pre- and postsynaptic activity profoundly changed the short-term plasticity and slowed the recovery from short-term depression. Synapse potentiation via stimulation of the cAMP or DAG pathway resulted in very similar changes. Fitting short-term plasticity models to the experimental data indicates that presynaptic LTP at cortical layer 5 input synapses is mediated primarily by an increased abundance of fully-primed and slowly-recovering vesicles.

Pre- Versus Postsynaptic LTP at Neocortical Synapses. While presynaptic LTP at large hippocampal mossy fiber synapses is well established (54, 55), involvement of presynaptic mechanisms in the early expression of LTP has been questioned altogether for small synapses that exhibit postsynaptic NMDAR-dependent LTP induction (6). The finding that postsynaptically "silent" synapses can be rapidly transformed into functional synapses by insertion of AMPARs during LTP induction argued in favor for a primarily postsynaptic site of LTP expression (56–59). Activation of silent synapses has been described as a mechanism of synapse potentiation primarily in early development (56, 60, 61). Nonetheless, synapses lacking AMPA receptors, which can be unsilenced through Hebbian plasticity (62), have been shown to be present structurally beyond early development (63, 64). However, the changes in short-term plasticity reported here are difficult to explain by an "unsilencing" of dormant synapses unless one postulates that those unsilenced synapses exhibit a different short-term plasticity. Furthermore, AMPA receptor saturation and desensitization are unlikely to be involved because they did not contribute to short-term plasticity in layer 5 pyramidal cells, neither under control conditions (*SI Appendix*, Fig. S3) nor under elevated p_{vr} conditions (52). Importantly, our data do not rule out a contribution of postsynaptic mechanisms to LTP expression at layer 5 synapses. Indeed, a small increase in the size of spontaneously occurring EPSCs was observed following pharmacological induction of LTP (Fig. 5*C*), which is likely of postsynaptic origin. However, the most parsimonious explanation for LTP-induced changes of short-term plasticity and recovery from short-term depression is a presynaptic mechanism, which is consistent with previous studies demonstrating a presynaptic component of LTP at small synapses in the CA1 region of the hippocampus (28, 65, 66) and the neocortex (10, 11).

Under our experimental conditions, some synapses did not show EPSC potentiation after stimulation with the LTP induction protocol (non-inducible connections). Individual synaptic connections may differ in their ability to potentiate depending on their initial properties (15, 67–72). However, we could not detect a correlation between initial synaptic strength or short-term plasticity parameters and the amount of LTP (*SI Appendix*, Fig. S1*C*), suggesting that in our experiments, the propensity to potentiate was independent of synaptic short-term plasticity parameters before induction.

Among possible technical explanations accounting for a failure of LTP induction are insufficient triggering of LTP expression pathways, due to low postsynaptic depolarization levels (15), subthreshold dendritic calcium signals (13), or washout of postsynaptic cytosolic molecules required for triggering LTP (73). However, these technical reasons are unlikely the cause for our non-inducible connections. First, the level of somatic depolarization achieved during pairing in our recordings with extracellular input stimulation (n = 38) and L5-L5 pyramidal cell pairs (n = 10) were larger than 2.3 mV, which was shown to be a critical level for LTP induction (15). Second, our recording time before starting the induction protocol was less than the critical time of 30 min (73) and did not differ between inducible and non-inducible connections, suggesting a negligible role of LTP washout. Third, we also observed non-inducible connections following pharmacological induction of potentiation, arguing in favor of intrinsic differences among synapses with respect to their ability to get potentiated (other than the initial short-term plasticity parameters). Nevertheless, other technical aspects cannot be completely excluded, and further studies are needed to clarify the reasons why some synapses resisted to LTP induction under our experimental conditions.

A Subpopulation of Release-Ready Vesicles Mediates LTP. In principle, presynaptic LTP can be mediated by changes in the number of release sites, the number of release-ready vesicles, and p_{vr}. Even though Katz postulated the existence of release sites (N; ref. 74) already decades ago, estimating N experimentally is still complicated because not all release sites are necessarily occupied by a vesicle (75) and because of heterogeneities among release-ready

vesicles due to superpriming (32, 33) or differences in the docking state (24). At layer 5 pyramidal cell input synapses, the increased short-term depression upon LTP induction was accounted for previously by increased p_{vr} (9). Our analysis indicates alternative or additional mechanisms involving an increase in the number of release-ready vesicles. Consistent with our results in the neocortex, an increased number of docked and active zone-associated vesicles has been observed at small CA1 hippocampal synapses following electrical and pharmacological LTP induction (28, 65). Increases in the number of docked vesicles have also been observed at the larger hippocampal mossy fiber boutons following pharmacological (55) and posttetanic potentiation (76, 77), at cultured hippocampal synapses following silencing-induced homeostatic plasticity (78) and at cerebellar parallel fiber-Purkinje cell synapses following pharmacological activation of b-adrenergic receptors (79).

In addition to changes in the number of release-ready vesicles, we found a slowing of the recovery from short-term depression following LTP induction (Fig. 2 *H* and *I*). The slower recovery was mediated by a selective increase in the amplitude of the slow component of recovery, resulting in more synaptic connections with biexponential recovery time courses following LTP induction (Fig. 2*E*). Such change in the recovery time course is difficult to explain by a sole increase in p_{vr} and/or a larger number of release-ready vesicles. Instead, our data argue for a heterogeneity among release-ready vesicles as shown e.g., at hippocampal synapses (32, 80), calyx of Held synapses (33, 81, 82), the cerebellar mossy fiber boutons (46, 83), and neuromuscular junctions of drosophila (47) and of cray fish (84). We extend this concept by showing that release-ready vesicles also differ in their role for synaptic long-term potentiation. In particular, our data indicate that a subpopulation of vesicles, which are fully-primed and slowly-recovering, is up-regulated following LTP induction. Our functional analysis is consistent with a recent electron microscopic study at CA1 hippocampal synapses reporting that the density of tightly docked vesicles increased following LTP induction, whereas the density of loosely docked vesicles remained unchanged (28). It is therefore tempting to speculate that the vesicles with shorter tethers represent fully-primed vesicles (85), which recover slowly from short-term depression.

Why Is LTP Slowing the Recovery from Short-Term Depression? Considering that LTP represents a strengthening of synapses, a slower time course of recovery from synaptic short-term depression may seem counterintuitive because it weakens synapses during repetitive activation. In principle, this could be "a bug or a feature." The slower recovery after LTP may be beneficial for the information flow in a neuronal network beyond a mere strengthening of synaptic weights (16, 86, 87) Alternatively, it may reflect a biophysical limitation imposed by the time required to build up the mature release machinery of the fully-primed vesicles under resting conditions.

A recent study inducing LTP at hippocampal mossy fiber boutons with optogenetic stimulation found an increased rate of vesicle replenishment (88). This apparent discrepancy with the slower recovery from short-term depression measured after cessation of stimulation as reported here can be understood as follows. In the study by Fukaya et al. (88), release was assessed with repetitive 20-ms depolarizations and capacitance measurements. This technique provides the absolute rate of vesicle replenishment per bouton during activity. It is the product of the number of release-ready vesicles and the recruitment rate per vesicle and determines the steady-state EPSC amplitude during high-frequency transmission (cf. Box 1 in ref. 44). Indeed, we observed similarly elevated steady-state EPSC amplitudes in potentiated synapses (Fig. 2*D*) indicating that LTP increased the absolute rate of vesicle replenishment during activity at neocortical synapses. Heterogeneities among release-ready vesicles and the activity dependence of vesicle replenishment provide additional explanations for a more prominent slow EPSC recovery component at rest despite enhanced vesicle replenishment during synapse activity.

Priming during LTP and pharmacological potentiation. Our data favor a mechanism postulating a shift in the balance of vesicle priming states underlying LTP. To test our hypothesis of enhanced vesicle priming, we used pharmacological tools, which stimulate active zone proteins known to facilitate vesicle priming. Munc13 is a key priming factor of synaptic vesicles exhibiting several regulatory domains including the C1 domain which binds DAG and can be activated by DAG analogues, such as the phorbol ester PDBu (89–92). Furthermore, the C2A domain of Munc13 can be activated through its interaction with RIM1α (93–96) and RIM1α in turn can be activated by the protein kinase A/cAMP pathway (97–99), but see ref. 100. We therefore focused on the pharmacological activation of the DAG- and cAMP-pathway by PDBu and forskolin, respectively. We found striking similarities in the changes in short-term plasticity upon LTP induced by electrical stimulation compared to pharmacological stimulation of the cAMP or DAG pathways. Particularly, the augmented slow component of the recovery time course occurring upon both LTP and pharmacological stimulation of vesicle priming strongly supports our conclusion that LTP is mediated by enhanced vesicle priming.

The presynaptic molecular mechanisms operating during LTP are still not fully understood. Particularly, the time course and magnitude of cAMP and DAG elevation required for the expression of LTP are unknown and may differ between synapses. Indeed, a comparison of LTP and forskolin-induced potentiation revealed mechanistic differences regarding the involvement of Rab3 (101), RIM1α (98), PKA (102), Epac (79, 103–105), and Ca^{2+} channels (106, 107). However, we established a number of similarities between LTP and pharmacological synaptic potentiation, which may indicate a convergence of downstream pathways eventually activating Munc13.

Parallel Versus Sequential Mechanisms of Vesicle Priming. Although the kinetic schemes of the two previously established models of vesicle priming (Fig. 3*A* and *SI Appendix*, Fig. S5*A*) appear to be quite similar, there are fundamental mechanistic differences. Accordingly, both models differ slightly in their predictions about the mechanisms underlying LTP. The sequential model (34) assumes a constant number of release sites, which can be empty or occupied by vesicles in one of two states (LS or TS). Only TS vesicles are fusion-competent, and p_{vr} is considered identical for all TS vesicles. Transitions between states are reversible, Ca^{2+}-dependent, and may be quite fast. Variations in both synaptic strength and plasticity among synapses and also upon LTP induction are explained by different resting occupancies of LS and TS states, which are in a dynamic equilibrium with each other and the empty state. The parallel model (46), in contrast, assumes two types of release sites (N_1 and N_2), which vary in number among synapses and may change upon induction of LTP. The two types of release sites have distinct p_{vr} and priming kinetics, they are fully occupied at rest, and recruitment of vesicles to sites is Ca^{2+}-independent. Both models reproduce short-term plasticity at layer 5 pyramidal cell synapses across a large range of frequencies almost equally well (Fig. 3*B* and *SI Appendix*, Fig. S5*B*). The parallel model has the advantage of being intuitively tangible. The sequential model has the advantage of incorporating recent experimental evidence regarding reversibility of priming and incomplete occupancy of release sites (34, 108,

109), Ca^{2+}-dependence of vesicle recruitment (108, 110, 111), and varying degrees of tight apposition between vesicle and active zone membrane of morphologically docked vesicles (26, 27). One of the main differences between both models is that the parallel model predicts an increased number of N_2 sites upon LTP, while the sequential model predicts no change in the number of release sites but only changes in the balance of priming states of docked vesicles upon LTP, for which the regulatory domains of Munc13 offer several possibilities (24, 92).

Within the parallel-model framework, the recently described increased release probability during LTP at hippocampal mossy fiber boutons (88) is consistent with our findings because the presynaptic capacitance measurements used in that study report the increased average p_{vr} of N_1 and N_2 vesicles. For the same reason the sequential model, in which only TS vesicles are fusion-competent, can reproduce the LTP-induced changes in synaptic strength and plasticity on the basis of a shift from LS to TS without requiring a change in p_{vr}. Thus, both models are consistent with the existence of release sites with high p_{vr} (52) and rapid vesicle supply pools (112), as described at mature layer 5 pyramidal cell input synapses. Further studies are needed to differentiate unequivocally between the two models. Nevertheless, it is reassuring that two models with profoundly different underlying mechanisms both support our main conclusion that fully-primed and slowly-recovering vesicles mediate LTP.

In summary, our study combined recent evidence for multistep processes of vesicle priming with detailed quantitative dissection of the mechanisms of presynaptic LTP. We show that an increase of a subpopulation of vesicles mediates LTP. These vesicles exhibit a fully matured priming state, a slow recovery from short-term depression, and presumably a tight docking state with short vesicle tethering filaments (28).

Methods

Full methods are available in *SI Appendix*.

Animals. Animals were handled in accordance with European (EU Directive 2010/63/EU, Annex IV for animal experiments), national and Leipzig University guidelines. All experiments were approved in advance by the federal Saxonian Animal Welfare Committee (T29/19). Patch-clamp recordings were made from neocortical layer 5 pyramidal cells and hippocampal CA1 pyramidal cells in acute brain slices obtained from Sprague Dawley rats of either sex at postnatal (P) day P13-P21.

Electrophysiology. Postsynaptic whole-cell recordings were obtained from visually identified layer 5 pyramidal neurons in the rat somatosensory cortex S1 region, from pyramidal cells in the CA1 region of the hippocampus in acute brain slices, and from cultured neocortical neurons using an EPC 10 USB amplifier (HEKA Elektronik). Pipette solution for voltage-clamp recordings in acute brain slices contained (in mM) 130 $KMeSO_3$, 10 KCl, 10 HEPES, 0.1 EGTA, 3 Mg-ATP, 0.3 Na-GTP, and 5 Na-phosphocreatine, pH adjusted to 7.31 by KOH and osmolarity to 294 mOsm by sucrose. Pipette solution for voltage-clamp recordings of EPSCs in cultured neurons contained (in mM) 150 K-Gluconate, 10 K-HEPES, 3 Mg-ATP, 0.3 Na-GTP, 0.05 EGTA, 10 NaCl, and 3 QX 314-Cl, pH adjusted to 7.35 by KOH, and osmolarity 295 mOsm. Pipette solution for voltage-clamp recordings of IPSCs in cultured neurons contained (in mM) 40 CsCl, 10 HEPES, 90 K-gluconate, 0.05 EGTA, 10 Na-phosphocreatine, 1.8 NaCl, 2 MgATP, 0.4 Na_2-GTP, 1.7 $MgCl_2$, 3.5 KCl, and 3 QX314-Cl, pH adjusted to 7.35 by CsOH, and osmolarity 297 mOsm.

Recordings in acute brain slices were obtained using artificial cerebrospinal fluid (ACSF) solution as described above. In a subset of experiments, ACSF was supplemented with the low-affinity AMPAR antagonist γDGG (2 to 3 mM) to attenuate postsynaptic saturation and desensitization. Recordings in cultured neurons were obtained using an external solution containing (in mM) 150 NaCl, 4 KCl, 10 HEPES, 10 glucose, 1.1 $MgCl_2$, and 1.1 $CaCl_2$, pH adjusted to 7.4 by NaOH at 35 °C, and osmolarity 305 mOsm. For all experiments, external solution was supplemented with blockers of NMDARs (20 μM APV) and $GABA_B$Rs (3 μM CGP-55845). For recordings of AMPAR-mediated EPSCs, external solution was supplemented with the $GABA_A$R antagonist SR95531 (10 μM) and the low-affinity GluR antagonist kynurenic acid (1 mM). For recordings of $GABA_A$R-mediated IPSCs, the external solution was supplemented with the AMPAR antagonist NBQX (20 μM) and the low-affinity $GABA_A$R antagonist TPMPA (0.3 mM).

Pipettes were pulled from borosilicate glass with open-tip resistance between 3 to 5 MΩ. For recordings in acute brain slices, the series resistance (R_s) was monitored and R_s compensation was dynamically adjusted every 2 min to yield a remaining uncompensated R_s of 10 MΩ (mean initial R_s values without compensation were 11.9 ± 2.9 MΩ, n = 54). Neurons were held in voltage-clamp mode at a membrane voltage (V_m) of −70 mV during pre- and post-LTP induction recording periods. Voltage-clamp recordings were sampled at 20 to 100 kHz and low-pass filtered at 3.9 kHz.

Spontaneous EPSCs (sEPSCs, Fig. 5 *B* and *C*) were measured without stimulation of excitatory inputs and in the absence of TTX. sEPSCs thus possibly represent a mixture of postsynaptic responses generated by spontaneous fusion of single vesicles (miniature EPSCs) and by vesicle release elicited by spontaneously occurring presynaptic action potentials.

Excitatory Input Stimulation at Layer 5 Pyramidal Cell Synapses. Excitatory postsynaptic currents (EPSCs) were evoked by extracellular stimulation in the vicinity of basal dendrites of layer 5 pyramidal cells (PCs) within layer 5 using a (ISO-Pulser ISOP1, AD-Elektronik, Buchenbach, Germany). Inputs were stimulated repetitively with a pattern consisting of a train of 30 pulses at 50 Hz followed by single pulses at different interstimulus intervals to probe recovery. Finally, 20 s after the 50 Hz train, a pair of stimuli with an interstimulus interval of 20 ms was delivered (Fig. 1*B*). This stimulus pattern (train + paired-pulses) was repeated every 45 s for ~10 min before LTP induction (before LTP baseline period) and up to 25 min after LTP induction (after LTP baseline period), also referred to as early LTP or short-term potentiation (113, 114). To isolate EPSCs, V_m was set close to the Cl^--equilibrium potential (approximately −69 mV). Bath application of SR95531 induced hyperactivity during recordings and was therefore not applicable. In a subset of experiments, 20 μM SR95531 were locally pressure applied via the stimulation electrode to block local $GABA_A$ receptors. LTP-induced changes in EPSC size and short-term plasticity were not significantly different between cells with and without local blockade of $GABA_A$ receptors (*SI Appendix*, Fig. S8), and data were therefore pooled. For comparisons before and after LTP induction, EPSCs during the last 9 min before induction ("before" LTP condition) and all EPSCs after induction ("after" LTP condition) were analyzed.

For paired recordings of synaptically connected layer 5 pyramidal cells (*SI Appendix*, Fig. S2), presynaptic cells were stimulated by 1.5 ms long voltage steps in on-cell (200–400 mV) or whole-cell (100 mV) configuration as described previously (52, 112). Stimulation-triggered EPSCs were recorded in postsynaptic pyramidal cells in whole-cell configuration.

LTP Induction at Layer 5 Pyramidal Cell Synapses. To elicit electrically induced LTP, pre- and postsynaptic activity was paired in current current-clamp mode and the bridge balance was set to 100%. The LTP induction protocol consisted of 30 pre-post pairings at 0.1 Hz (Fig. 1*B*). Presynaptic activity was elicited by extracellular stimulation of the inputs (8 pulses at 50 Hz) and was paired with a 2 ms delayed postsynaptic depolarization induced by a 200 ms long current injection into the postsynaptic cell to evoke AP firing (9, 10). The amplitude of the injected current was adjusted to achieve an AP firing frequency ≥35 Hz. Presynaptic stimulation and postsynaptic APs were not precisely timed. In between pairings, V_m of the postsynaptic cell was adjusted to approximately −70 mV.

Pharmacological Induction of Vesicular Release Potentiation. For pharmacological induction of EPSC potentiation (Figs. 4*H* and 5), forskolin and PDBu were first dissolved in DMSO and further diluted in ACSF to a final concentration of 40 μM and 1 μM, respectively. After establishing the before-LTP-induction (baseline) period (see above), forskolin or PDBu containing ACSF was washed in through the perfusion system while continuing input stimulation. To assess the effects of the drugs, EPSCs recorded after 4.5 min of wash-in were analysed. To exclude possible effects of DMSO onto synaptic strength, control ACSF was supplemented with an identical amount of DMSO (≤0.1%) as forskolin- or PDBu-containing ACSF.

Statistics. All pairwise comparisons between values before and after LTP induction were done by Wilcoxon signed-rank tests. For unpaired comparisons between inducible and non-inducible connections, Mann–Whitney rank-sum

tests were applied. For the multiple comparisons in Fig. 1*F*, Kruskal–Wallis one-way ANOVA on ranks was performed followed by Dunn's post hoc pairwise tests. All correlations (Figs. 4 and 5 and *SI Appendix*, Fig. S2) were tested for statistical significance using Spearman's rank order correlation tests (r_s denotes the corresponding correlation coefficient). All values are presented as median [first quartile, third quartile] if not stated otherwise. Statistical tests were performed with jamovi (https://www.jamovi.org).

Data, Materials, and Software Availability. C++ code for numerical simulations is available at https://github.com/HallermannLab/2023_PNAS (45). All other data are included in the article and *SI Appendix*.

ACKNOWLEDGMENTS. We thank Dr. Takeshi Sakaba for valuable discussions and comments on the manuscript. This work was supported by the Deutsche Forschungsgemeinschaft (DFG, German Research Foundation; HA6386/10-1 to S.H.; SCHM1838/4-1 to H.S.; Collaborative Research Center 1286 "Quantitative Synaptology," E.N. and H.T.) and under Germany's Excellence Strategy (EXC 2067/1-390729940, E.N.) and by a European Research Council Consolidator Grant (ERC CoG 865634 to S.H.). R.J.K. is a member of the DFG KFO 5001 ResolvePAIN, Project ID 426503586.

Author affiliations: [a]Faculty of Medicine, Carl-Ludwig-Institute for Physiology, Leipzig University, Leipzig 04103, Germany; [b]Department of Molecular Neurobiology, Max Planck Institute for Multidisciplinary Sciences, Göttingen 37075, Germany; [c]Department of Animal Physiology, Institute of Biology, Leipzig University, Leipzig 04103, Germany; [d]Emeritus Laboratory of Membrane Biophysics, Max Planck Institute for Multidisciplinary Sciences, Göttingen 37070, Germany; and [e]Cluster of Excellence "Multiscale Bioimaging: From Molecular Machines to Networks of Excitable Cells", University of Göttingen, Göttingen 37073, Germany

1. S. J. Martin, P. D. Grimwood, R. G. M. Morris, Synaptic plasticity and motor learning: An evaluation of the hypothesis. *Annu. Rev. Neurosci.* **23**, 649–711 (2000).
2. H. R. Monday, T. J. Younts, P. E. Castillo, Long-term plasticity of neurotransmitter release: Emerging mechanisms and contributions to brain function and disease. *Annu. Rev. Neurosci.* **41**, 299–322 (2018).
3. R. D. Hawkins, E. R. Kandel, S. A. Siegelbaum, Learning to modulate transmitter release: Themes and variations in synaptic plasticity. *Annu. Rev. Neurosci.* **16**, 625–665 (1993).
4. P. E. Castillo, Presynaptic LTP and LTD of excitatory and inhibitory synapses. *Cold Spring Harb. Perspect. Biol.* **4**, 5728–5729 (2012).
5. Y. Yang, N. Calakos, Presynaptic long-term plasticity. *Front. Synaptic Neurosci.* **5**, 8 (2013).
6. R. A. Nicoll, A brief history of long-term potentiation. *Neuron* **93**, 281–290 (2017).
7. R. Enoki, Y. L. Hu, D. Hamilton, A. Fine, Expression of long-term plasticity at individual synapses in hippocampus is graded, bidirectional, and mainly presynaptic: Optical quantal analysis. *Neuron* **62**, 242–253 (2009).
8. T. V. P. Bliss, G. L. Collingridge, Expression of NMDA receptor-dependent LTP in the hippocampus: Bridging the divide. *Mol. Brain* **6**, 1–14 (2013).
9. H. Markram, M. Tsodyks, Redistribution of synaptic efficacy between neocortical pyramidal neurons. *Nature* **382**, 807–810 (1996).
10. J. Sjöström, G. G. Turrigiano, S. B. Nelson, Multiple forms of long-term plasticity at unitary neocortical layer 5 synapses. *Neuropharmacology* **52**, 176–84 (2007).
11. M. Eder, W. Zieglgänsberger, H. U. Dodt, Neocortical long-term potentiation and long-term depression: Site of expression investigated by infrared-guided laser stimulation. *J. Neurosci.* **22**, 7558–7568 (2002).
12. H. Markram, J. Lübke, M. Frotscher, B. Sakmann, Regulation of synaptic efficacy by coincidence of postsynaptic APs and EPSPs. *Science* **275**, 213–215 (1997).
13. B. M. Kampa, J. J. Letzkus, G. J. Stuart, Requirement of dendritic calcium spikes for induction of spike-timing-dependent synaptic plasticity. *J. Physiol.* **574**, 283–290 (2006).
14. J. A. D'amour, R. C. Froemke, Inhibitory and excitatory spike-timing-dependent plasticity in the auditory cortex. *Neuron* **86**, 514–528 (2015).
15. P. J. Sjöström, G. G. Turrigiano, S. B. Nelson, Rate, timing, and cooperativity jointly determine cortical synaptic plasticity. *Neuron* **32**, 1149–1164 (2001).
16. L. F. Abbott, S. B. Nelson, Synaptic plasticity: Taming the beast. *Nat. Neurosci.* **3**, 1178–1183 (2000).
17. P. S. Kaeser, W. G. Regehr, The readily releasable pool of synaptic vesicles. *Curr. Opin. Neurobiol.* **43**, 63–70 (2017).
18. A. Witkowska, L. P. Heinz, H. Grubmüller, R. Jahn, Tight docking of membranes before fusion represents a metastable state with unique properties. *Nat. Commun.* **12**, 2–8 (2021).
19. A. Witkowska, S. Spindler, R. G. Mahmoodabadi, V. Sandoghdar, R. Jahn, Differential diffusional properties in loose and tight docking prior to membrane fusion. *Biophys. J.* **119**, 2431–2439 (2020).
20. F. Michelassi, H. Liu, Z. Hu, J. S. Dittman, A C1–C2 module in Munc13 inhibits calcium-dependent neurotransmitter release. *Neuron* **95**, 577–590.e5 (2017).
21. N. Lipstein *et al.*, Munc13-1 is a Ca2+-phospholipid-dependent vesicle priming hub that shapes synaptic short-term plasticity and enables sustained neurotransmission. *Neuron* **109**, 1–21 (2021).
22. M. Camacho *et al.*, Control of neurotransmitter release by two distinct membrane-binding faces of the munc13-1 c1c2b region. *Elife* **10**, 1–34 (2021).
23. B. Quade *et al.*, Membrane bridging by munc13-1 is crucial for neurotransmitter release. *Elife* **8**, 1–30 (2019).
24. E. Neher, N. Brose, Dynamically primed synaptic vesicle states: Key to understand synaptic short-term plasticity. *Neuron* **100**, 1283–1291 (2018).
25. M. Silva, V. Tran, A. Marty, Calcium-dependent docking of synaptic vesicles. *Trends Neurosci.* **44**, 1–14 (2021).
26. S. Chang, T. Trimbuch, C. Rosenmund, Synaptotagmin-1 drives synchronous Ca 2+ -triggered fusion by C 2 B-domain-mediated synaptic-vesicle-membrane attachment. *Nat. Neurosci.* **21**, 33–42 (2018).
27. C. Imig *et al.*, The morphological and molecular nature of synaptic vesicle priming at presynaptic active zones. *Neuron* **84**, 416–431 (2014).
28. J. H. Jung, L. M. Kirk, J. N. Bourne, K. M. Harris, Shortened tethering filaments stabilize presynaptic vesicles in support of elevated release probability during LTP in rat hippocampus. *Proc. Natl. Acad. Sci. U.S.A.* **118**, 1–8 (2021).
29. T. Miki *et al.*, Actin- and myosin-dependent vesicle loading of presynaptic docking sites prior to exocytosis. *Neuron* **91**, 808–823 (2016).
30. M. Aldahabi *et al.*, Different priming states of synaptic vesicles underlie distinct release probabilities at hippocampal excitatory synapses. *Neuron* **110**, 4144–4161 (2022).
31. E. Hanse, B. Gustafsson, Vesicle release probability and pre-primed pool at glutamatergic synapses in area CA1 of the rat neonatal hippocampus. *J. Physiol.* **531**, 481–493 (2001).
32. O. M. Schlüter, J. Basu, T. C. Südhof, C. Rosenmund, Rab3 superprimes synaptic vesicles for release: Implications for short-term synaptic plasticity. *J. Neurosci.* **26**, 1239–1246 (2006).
33. H. Taschenberger, A. Woehler, E. Neher, Superpriming of synaptic vesicles as a common basis for intersynapse variability and modulation of synaptic strength. *Proc. Natl. Acad. Sci. U.S.A.* **113**, E4548–E4557 (2016).
34. K.-H. Lin, H. Taschenberger, E. Neher, A sequential two-step priming scheme reproduces diversity in synaptic strength and short-term plasticity. *Proc. Natl. Acad. Sci. U.S.A.* 119, e2207987119 (2022).
35. A. Rozov, J. Jerecic, B. Sakmann, N. Burnashev, AMPA receptor channels with long-lasting desensitization in bipolar interneurons contribute to synaptic depression in a novel feedback circuit in layer 2/3 of rat neocortex. *J. Neurosci.* **21**, 8062–8071 (2001).
36. A. Rozov, N. Burnashev, Polyamine-dependent facilitation of postsynaptic AMPA receptors counteracts paired-pulse depression. *Nature* **401**, 594–598 (1999).
37. J. I. Wadiche, C. E. Jahr, Multivesicular release at climbing fiber-purkinje cell synapses. *Neuron* **32**, 301–313 (2001).
38. L. O. Trussell, S. Zhang, I. M. Ramant, Desensitization of AMPA receptors upon multiquantal neurotransmitter release. *Neuron* **10**, 1185–1196 (1993).
39. X. Lou, V. Scheuss, R. Schneggenburger, Allosteric modulation of the presynaptic Ca2+ sensor for vesicle fusion. *Nature* **435**, 497–501 (2005).
40. S. Chanda, M. A. Xu-Friedman, A low-affinity antagonist reveals saturation and desensitization in mature synapses in the auditory brain stem. *J. Neurophysiol.* **103**, 1915–1926 (2010).
41. J. J. Crowley, A. G. Carter, W. G. Regehr, Fast vesicle replenishment and rapid recovery from desensitization at a single synaptic release site. *J. Neurosci.* **27**, 5448–5460 (2007).
42. A. Y. C. Wong, B. P. Graham, B. Billups, I. D. Forsythe, Distinguishing between presynaptic and postsynaptic mechanisms of short-term depression during action potential trains. *J. Neurosci.* **23**, 4868–4877 (2003).
43. E. Neher, Merits and limitations of vesicle pool models in view of heterogeneous populations of synaptic vesicles. *Neuron* **87**, 1131–1142 (2015).
44. S. Hallermann, R. A. Silver, Sustaining rapid vesicular release at active zones: Potential roles for vesicle tethering. *Trends Neurosci.* **36**, 185–194 (2013).
45. S. Hallermann, 2023_PNAS. GitHub. https://github.com/HallermannLab/2023_PNAS. Deposited 29 September 2023.
46. S. Hallermann *et al.*, Bassoon speeds vesicle reloading at a central excitatory synapse. *Neuron* **68**, 710–723 (2010).
47. S. Hallermann, M. Heckmann, R. J. Kittel, Mechanisms of short-term plasticity at neuromuscular active zones of Drosophila. *HFSP J.* **4**, 72–84 (2010).
48. A. Ritzau-Jost *et al.*, Apparent calcium dependence of vesicle recruitment. *J. Physiol.* **596**, 4693–4707 (2018).
49. E. Pofantis, E. Neher, T. Dresbach, Regulation of a subset of release-ready vesicles by the presynaptic protein Mover. *Proc. Natl. Acad. Sci. U.S.A.* **118**, 1–9 (2021).
50. C. Keine *et al.*, Presynaptic Rac1 controls synaptic strength through the regulation of synaptic vesicle priming. *Elife* **11**, e81505 (2022).
51. T. Branco, K. Staras, The probability of neurotransmitter release: Variability and feedback control at single synapses. *Nat. Rev. Neurosci.* **10**, 373–383 (2009).
52. G. Bornschein, J. Eilers, H. Schmidt, Neocortical high probability release sites are formed by distinct Ca2+ channel-to-release sensor topographies during development. *Cell Rep.* **28**, 1410–1418.e4 (2019).
53. E. T. Kavalali, The mechanisms and functions of spontaneous neurotransmitter release. *Nat. Rev. Neurosci.* **16**, 5–16 (2015).
54. R. A. Nicoll, D. Schmitz, Synaptic plasticity at hippocampal mossy fibre synapses. *Nat. Rev. Neurosci.* **6**, 863–876 (2005).
55. M. Orlando *et al.*, Recruitment of release sites underlies chemical presynaptic potentiation at hippocampal mossy fiber boutons. *PLoS Biol.* **19**, 1–29 (2021).
56. J. T. R. Isaac, R. A. Nicoll, R. C. Malenka, Evidence for silent synapses: Implications for the expression of LTP. *Neuron* **15**, 427–434 (1995).
57. D. Liao, R. H. Scannevin, R. Huganir, Activation of silent synapses by rapid activity-dependent synaptic recruitment of AMPA receptors. *J. Neurosci.* **21**, 6008–6017 (2001).
58. D. Liao, N. A. Hessler, R. Malinow, Activation of postsynaptically silent synapses during pairing-induced LTP in CA1 region of hippocampal slice. *Nature* **375**, 400–404 (1995).
59. J. M. Montgomery, P. Pavlidis, D. V. Madison, Pair recordings reveal all-silent synaptic connections and the postsynaptic expression of long-term potentiation. *Neuron* **29**, 691–701 (2001).
60. D. Liao, R. Malinow, Deficiency in induction but not expression of LTP in hippocampal slices from young rats. *Learn. Mem.* **3**, 138–149 (1996).
61. G. A. Kerchner, R. A. Nicoll, Silent synapses and the emergence of a postsynaptic mechanism for LTP. *Nat. Rev. Neurosci.* **9**, 813–825 (2008).
62. D. Vardalaki, K. Chung, M. T. Harnett, Filopodia are a structural substrate for silent synapses in adult neocortex. *Nature* **612**, 323–327 (2022).

63. Y. Takumi, V. Ramírez-León, P. Laake, E. Rinvik, O. P. Ottersen, Different modes of expression of AMPA and NMDA receptors in hippocampal synapses. *Nat. Neurosci.* **2**, 618–624 (1999).
64. Z. Nusser *et al.*, Cell type and pathway dependence of synaptic AMPA receptor number and variability in the hippocampus. *Neuron* **21**, 545–559 (1998).
65. S. Rey, V. Marra, C. Smith, K. Staras, Nanoscale remodeling of functional synaptic vesicle pools in hebbian plasticity. *Cell Rep.* **30**, 2006–2017.e3 (2020).
66. S. S. Zakharenko, L. Zablow, S. A. Siegelbaum, Visualization of changes in presynaptic function during long-term synaptic plasticity. *Nat. Neurosci.* **4**, 711–717 (2001).
67. D. Liao, A. Jones, R. Malinow, Direct measurement of quantal changes underlying long-term potentiation in CA1 hippocampus. *Neuron* **9**, 1089–1097 (1992).
68. G. Q. Bi, M. M. Poo, Synaptic modifications in cultured hippocampal neurons: Dependence on spike timing, synaptic strength, and postsynaptic cell type. *J. Neurosci.* **18**, 10464–10472 (1998).
69. D. Debanne, B. H. Gähwiler, S. M. Thompson, Heterogeneity of synaptic plasticity at unitary CA3-CA1 and CA3–CA3 connections in rat hippocampal slice cultures. *J. Neurosci.* **19**, 10664–10671 (1999).
70. P. E. Schulz, Long-term potentiation involves increases in the probability of neurotransmitter release. *Proc. Natl. Acad. Sci. U.S.A.* **94**, 5888–5893 (1997).
71. N. R. Hardingham, G. E. Hardingham, K. D. Fox, J. J. B. Jack, Presynaptic efficacy directs normalization of synaptic strength in layer 2/3 rat neocortex after paired activity. *J. Neurophysiol.* **97**, 2965–2975 (2007).
72. Y. P. Zhang, T. G. Oertner, Optical induction of synaptic plasticity using a light-sensitive channel. *Nat. Methods* **4**, 139–141 (2007).
73. R. Malinow, R. W. Tsien, Presynaptic enhancement shown by whole-cell recordings of long-term potentiation in hippocampal slices. *Nature* **346**, 177–180 (1990).
74. J. del Castillo, B. Katz, Statistical factors involved in neuromuscular facilitation and depression. *J Physiol.* **24**, 574–585 (1954).
75. C. Pulido, A. Marty, Quantal fluctuations in central mammalian synapses: Functional role of vesicular docking sites. *Physiol. Rev.* **97**, 1403–1430 (2017).
76. C. Imig *et al.*, Ultrastructural imaging of activity-dependent synaptic membrane-trafficking events in cultured brain slices. *Neuron* **108**, 843–860.e8 (2020).
77. D. Vandael, C. Borges-Merjane, X. Zhang, P. Jonas, Short-term plasticity at hippocampal mossy fiber synapses is induced by natural activity patterns and associated with vesicle pool engram formation. *Neuron* **107**, 509–521.e7 (2020).
78. V. N. Murthy, T. Schikorski, C. F. Stevens, Y. Zhu, Inactivity produces increases in neurotransmitter release and synapse size. *Neuron* **32**, 673–682 (2001).
79. R. Martín *et al.*, β-adrenergic receptors/epac signaling increases the size of the readily releasable pool of synaptic vesicles required for parallel fiber LTP. *J. Neurosci.* **40**, 8604–8617 (2020).
80. V. N. Murthy, T. J. Sejnowski, C. F. Stevens, Heterogeneous release properties of visualized individual hippocampal synapses. *Neuron* **18**, 599–612 (1997).
81. T. Sakaba, E. Neher, Calmodulin mediates rapid recruitment of fast-releasing synaptic vesicles at a calyx-type synapse. *Neuron* **32**, 1119–1131 (2001).
82. J. S. Lee, W. K. Ho, E. Neher, S. H. Lee, Superpriming of synaptic vesicles after their recruitment to the readily releasable pool. *Proc. Natl. Acad. Sci. U.S.A.* **110**, 15079–15084 (2013).
83. A. Ritzau-Jost *et al.*, Ultrafast action potentials mediate kilohertz signaling at a central synapse. *Neuron* **84**, 152–163 (2014).
84. B. Pan, R. S. Zucker, A general model of synaptic transmission and short-term plasticity. *Neuron* **62**, 539–554 (2009).
85. R. Fernández-Busnadiego *et al.*, Quantitative analysis of the native presynaptic cytomatrix by cryoelectron tomography. *J. Cell Biol.* **188**, 145–156 (2010).
86. R. P. Costa, B. E. P. Mizusaki, P. J. Sjöström, M. C. W. van Rossum, Functional consequences of pre- and postsynaptic expression of synaptic plasticity. *Philos. Trans. R. Soc. B Biol. Sci.* **372**, 20160153 (2017).
87. J. S. Rothman, L. Cathala, V. Steuber, R. A. Silver, Synaptic depression enables neuronal gain control. *Nature* **457**, 1015–1018 (2009).
88. R. Fukaya *et al.*, Increased vesicle fusion competence underlies long- term potentiation at hippocampal mossy fiber synapses. *Sci. Adv.* **2**, 1–14 (2023).
89. A. Betz *et al.*, Munc13-1 is a presynaptic phorbol ester receptor that enhances neurotransmitter release. *Neuron* **21**, 123–136 (1998).
90. J. Basu, A. Betz, N. Brose, C. Rosenmund, Munc13-1 C1 domain activation lowers the energy barrier for synaptic vesicle fusion. *J. Neurosci.* **27**, 1200–1210 (2007).
91. J.-S. Rhee *et al.*, "Phorbol Ester-and Diacylglycerol-Induced Augmentation of Transmitter Release Is Mediated by Munc13s and Not by PKCs regions and involve successive, spatially segregated modulations of pre-and postsynaptic processes (Ma-lenka and Nicoll, 1999). Presynaptic" (2002).
92. J. S. Dittman, Unc13: A multifunctional synaptic marvel. *Curr. Opin. Neurobiol.* **57**, 17–25 (2019).
93. L. Deng, P. S. Kaeser, W. Xu, T. C. Südhof, RIM proteins activate vesicle priming by reversing autoinhibitory homodimerization of munc13. *Neuron* **69**, 317–331 (2011).
94. A. Betz *et al.*, Functional interaction of the active zone proteins Munc13-1 and RIM1 in synaptic vesicle priming. *Neuron* **30**, 183–196 (2001).
95. J. Lu *et al.*, Structural basis for a Munc13-1 homodimer to Munc13-1/RIM heterodimer switch. *PLoS Biol.* **4**, 1159–1172 (2006).
96. M. Camacho *et al.*, Heterodimerization of Munc13 C2A domain with RIM regulates synaptic vesicle docking and priming. *Nat. Commun.* **8**, 1–13 (2017).
97. E. Fourcaudot *et al.*, cAMP/PKA signaling and RIM1α mediate presynaptic LTP in the lateral amygdala. *Proc. Natl. Acad. Sci. U.S.A.* **105**, 15130–15135 (2008).
98. P. E. Castillo, S. Schoch, F. Schmitz, T. C. Südhof, R. C. Malenka, RIM1α is required for presynaptic long-term potentiation. *Nature* **415**, 327–330 (2002).
99. J. A. Müller *et al.*, A presynaptic phosphosignaling hub for lasting homeostatic plasticity. *Cell Rep.* **39**, 110696 (2022).
100. P. S. Kaeser *et al.*, "RIM1 phosphorylation at serine-413 by protein kinase A is not required for presynaptic long-term plasticity or learning" (2008).
101. P. E. Castillo *et al.*, Rab3A is essential for mossy fibre long-term potentiation in the hippocampus. *Nature* **388**, 590–593 (1997).
102. Y. Y. Huang *et al.*, Genetic evidence for a protein-kinase-A-mediated presynaptic component in NMDA-receptor-dependent forms of long-term synaptic potentiation. *Proc. Natl. Acad. Sci. U.S.A.* **102**, 9365–9370 (2005).
103. J. J. Ferrero *et al.*, β-adrenergic receptors activate exchange protein directly activated by cAMP (Epac), translocate munc13-1, and enhance the Rab3A-RIM1 α interaction to potentiate glutamate release at cerebrocortical nerve terminals. *J. Biol. Chem.* **288**, 31370–31385 (2013).
104. I. Gekel, E. Neher, Application of an Epac activator enhances neurotransmitter release at excitatory central synapses. *J. Neurosci.* **28**, 7991–8002 (2008).
105. X.-T. Wang *et al.*, cAMP−EPAC−PKC ε−RIM1 α signaling regulates presynaptic long-term potentiation and motor learning. *Elife* **12**, 1–29 (2023).
106. M. Midorikawa, T. Sakaba, Kinetics of releasable synaptic vesicles and their plastic changes at hippocampal mossy fiber synapses. *Neuron* **96**, 1033–1040.e3 (2017).
107. R. Fukaya, M. Maglione, S. J. Sigrist, T. Sakaba, Rapid Ca2+ channel accumulation contributes to cAMP-mediated increase in transmission at hippocampal mossy fiber synapses. *Proc. Natl. Acad. Sci. U.S.A.* **118**, 1–11 (2021).
108. G. Malagon, T. Miki, V. Tran, L. C. Gomez, A. Marty, Incomplete vesicular docking limits synaptic strength under high release probability conditions. *Elife* **9**, 1–18 (2020).
109. E. He *et al.*, Munc13-1 and Munc18-1 together prevent NSF-dependent de-priming of synaptic vesicles. *Nat. Commun.* **8**, 1–10 (2017).
110. A. Eshra, H. Schmidt, J. Eilers, S. Hallermann, Calcium dependence of neurotransmitter release at a high fidelity synapse. *Elife* **10**, 1–34 (2021).
111. N. Hosoi, T. Sakaba, E. Neher, Quantitative analysis of calcium-dependent vesicle recruitment and its functional role at the calyx of held synapse. *J. Neurosci.* **27**, 14286–14298 (2007).
112. G. Bornschein, S. Brachtendorf, H. Schmidt, Developmental increase of neocortical presynaptic efficacy via maturation of vesicle replenishment. *Front. Synaptic Neurosci.* **11**, 1–10 (2020).
113. K. M. Harris, Synaptic odyssey. *J. Neurosci.* **40**, 61–80 (2020).
114. U. Frey, R. G. M. Morris, Synaptic tagging and long-term potentiation. *Nature* **385**, 533–536 (1997).